Whole-brain mapping of increased manganese levels in welders and its association with exposure and motor function

Humberto Monsivais[a], Chien-Lin Yeh[a,b], Alex Edmondson[c,d], Roslyn Harold[e], Sandy Snyder[a,f], Ellen M. Wells[a,g], Tobias Schmidt-Wilcke[h,i], Dan Foti[e], S. Elizabeth Zauber[j], Ulrike Dydak[a,k,*]

[a]School of Health Sciences, Purdue University, West Lafayette, IN, USA

[b]Takeda Pharmaceutical Company Ltd, Cambridge, MA, USA

[c]Cincinnati Children's Hospital Medical Center, Imaging Research Center, Cincinnati, OH, USA

[d]University of Cincinnati College of Medicine, Department of Environmental and Public Health Sciences, Cincinnati, OH USA

[e]Department of Psychological Sciences, Purdue University, West Lafayette, IN, USA

[f]Department of Speech, Language and Hearing Sciences, Purdue University, West Lafayette, IN, USA

[g]Department of Public Health, Purdue University, West Lafayette, IN, USA

[h]Department of Neurology, St. Mauritius Therapieklinik, Meerbusch, Germany

[i]Institute of Clinical Neuroscience and Medical Psychology, Universitätsklinikum Düsseldorf, Düsseldorf, Germany

[j]Department of Neurology, Indiana University School of Medicine, Indianapolis, USA

[k]Department of Radiology and Imaging Sciences, Indiana University School of Medicine, Indianapolis, IN, USA

Abstract

Although manganese (Mn) is a trace metal essential for humans, chronic exposure to Mn can cause accumulation of this metal ion in the brain leading to an increased risk of neurological and neurobehavioral health effects. This is a concern for welders exposed to Mn through welding fumes. While brain Mn accumulation in occupational settings has mostly been reported in the basal ganglia, several imaging studies also revealed elevated Mn in other brain areas. Since Mn functions as a magnetic resonance imaging (MRI) T1 contrast agent, we developed a whole-brain MRI approach to map *in vivo* Mn deposition differences in the brains of non-exposed factory controls and exposed welders. This is a cross-sectional analysis of 23 non-exposed factory controls and 36 exposed full-time welders from the same truck manufacturer. We collected high-resolution 3D MRIs of brain anatomy and R1 relaxation maps to identify regional differences using voxel-based quantification (VBQ) and statistical parametric mapping. Furthermore, we investigated the associations between excess Mn deposition and neuropsychological and motor test performance. Our results indicate that: (1) Using whole-brain MRI relaxometry methods we can generate excess Mn deposition maps *in vivo*, (2) excess Mn accumulation due to occupational exposure occurs beyond the basal ganglia in cortical areas associated with motor and cognitive functions, (3) Mn likely diffuses along white matter tracts in the brain, and (4) Mn deposition in specific brain regions is associated with exposure (cerebellum and frontal cortex) and motor metrics (cerebellum and hippocampus).

Keywords

1. Introduction

Manganese (Mn) is an essential trace metal for humans required for numerous indispensable biochemical processes throughout the human body including regulation of energy consumption, growth, coagulation, hemostatic function, and removal of by-products of aberrant oxidative stress (Aschner and Erikson, 2017). However, Mn is also neurotoxic at high doses and poses a health concern to thousands of welders who inhale welding fumes in the manufacturing industry.

High exposure to Mn can lead to motor symptoms such as bradykinesia, dystonia, tremor and rigidity, (Guilarte and Gonzales, 2015; Racette et al., 2012; Tsuboi et al., 2007) as well as cognitive and neurobehavioral deficits (Bowler et al., 2006; Bowler et al., 2007; Bowler and Lezak, 2015; Bowler et al., 2018; Zoni et al., 2007; Martin et al., 2020). These motor and cognitive symptoms are summarized under the term "manganism" (Crossgrove and Zheng, 2004) a parkinsonian like disorder. Motor symptoms do not recede upon cessation of exposure (Guilarte, 2013) and typically do not improve with the standard treatment for Parkinson's disease, levodopa (Olanow, 2004). Therefore, screening tools to assess welders who are at risk of Mn toxicity before any symptoms develop are imperative.

Due to the strong paramagnetism of Mn, it serves as a contrast agent in magnetic resonance imaging (MRI) by shortening the longitudinal relaxation time T1, or respectively increasing the relaxation rate R1 (R1 = 1/T1). Therefore, lower relaxation times result in higher signal

intensities ("hyperintensities") in T1-weighted (T1-w) imaging. In Mn-exposed workers, a signal intensity index called the pallidal index (PI), which represents the ratio of T1-w signal intensity in the globus pallidus (GP) relative to the signal intensity in frontal white matter (FWM) (Krieger et al., 1995), has been shown to be correlated to markers of exposure such as blood Mn concentration (Chang et al., 2010; Jiang et al., 2007), cumulative exposure indexes (Dietz et al., 2001), and neurobehavioral performance (Shin et al., 2007). However, the validity of the PI in reflecting brain Mn levels is only accurate in a limited range due to increased Mn accumulation in the WM with increased Mn exposure (Guilarte et al., 2006). Studies investigating Mn-exposed non-human primates showed an accumulation of Mn in the white matter and the cortex (Guilarte et al., 2006). The involvement of cortical structures was also demonstrated in an animal study, where Mn was observed to induce microstructure damage in the frontal white matter (Verina et al., 2013). These results indicate that the PI may be less descriptive of an imaging marker for assessing the concentration of Mn in the brain. Therefore, a direct measurement of the T1 relaxation time, known as T1 mapping, may be more sensitive to brain Mn levels.

Early studies assessing the T1 relaxation time in the human brain employed long acquisition times and were limited to a specific brain region. For example, Sen et al. (2011) focused on measuring R1 (R1 = 1/T1) in the olfactory bulb to study Mn accumulation in asymptomatic welders, while Choi et al. (2007) focused on the GP only. However, the recent development of fast and generally robust T1 mapping imaging techniques allow for voxel-wise quantification of T1 throughout the whole brain. Several studies have used T1 mapping to study the uptake, accumulation, and dispersion of Mn in the brain of welders (Ma et al., 2018; Lee et al., 2018; Lee et al., 2015; Edmondson et al., 2019; Lewis et al., 2016; Long et al., 2015); however, most of them have concentrated on the basal ganglia structures only by employing the commonly used region of interest (ROI) analysis approach. While this approach is valid to answer specific questions, it only provides selective regional information and potentially misses important information from outside of the ROI.

Because Mn can disperse throughout the brain, we developed a sensitive, whole-brain imaging approach to better understand the spatial distribution of Mn throughout the entire human brain. We hypothesize that R1 is highly sensitive to Mn deposition, and thus can reliably measure the accumulation of Mn beyond the basal ganglia, including in cortical and cerebellar regions and white matter tracts, even under the condition of low-level exposure such as in an occupational setting. Overall, we aimed to provide a rigorous tool to detect and visualize elevated Mn levels at a whole-brain level and a measure that enables the study of correlations of Mn exposure with neurotoxic effects and the differential involvement of different brain regions.

2. Methods

2.1. Study design and subjects

Forty-six (46) full-time steel-welders (mean age ± SD: 41 ± 10 years, range: 21–61 years) were recruited from a US truck-trailer manufacturer. Thirty-four (34) frequency age-matched workers (mean age ± SD: 39 ± 12 years, range: 20–61 years), who were not exposed to welding fumes and worked as assembly workers or similar, were recruited

as a control group from the same factory. The research received approval from Purdue University's Institutional Review Board (Protocol #: 1205012374), and all participants provided written informed consent before taking part in the study. Inclusion criteria included male sex, age   18 years, and employed by the trailer manufacturer for at least 3 years; for this analysis subjects were also limited to those who had a complete good quality MRI and provided a complete medical and work history questionnaire. Subjects with a history of PD or other motor disorders were excluded from participation. More details about the study have been published previously (Ma et al., 2018; Ward et al., 2018). The study was completed in 2016; this analysis includes cross-sectional data collected from February 2013–May 2016 (see Supplementary Material for detailed characteristics of all study participants).

Four welders and seven controls could not complete the MRI exam due to claustrophobia. Three MRI sets from the welder group and one from the control group were excluded due to bad image quality. Further, three more welders were excluded due to limited welding time (i.e., supervisors). Lastly, three controls were disqualified due to having part-time welding experience (i.e., were welding at the time of MRI acquisition). Thus, a total of 36 welders and 23 controls were included in all further analyses presented in this paper (see Table 1 for detailed characteristics of participants for this study).

2.2. Exposure, neurological and neuropsychological assessment

Subjects completed questionnaires to obtain information on demographics (age, education, anthropometrics), medical history, and work history. We used an exposure model (Ward et al., 2018) to estimate each subject's Mn cumulative exposure index (CEI) over different time intervals. Briefly, the model uses personal air samples, combined with a detailed work history of each subject and weighting factors for specific conditions such as wearing a respirator. Selected time intervals included exposure over the past-3-months (Mn – CEI_{3M}) before MRI, past 7-12 months before MRI (Mn – $CEI_{7–12M}$), and cumulative exposure since age 18 (Mn – CEI_{Life}).

A certified neurologist (S.E.Z.) with expertise in movement disorders scored each subject's (welders and controls) motor function using the Unified Parkinson's Disease Rating Scale (UPDRS) (Goetz et al., 2008). In addition, cognitive testing was performed by trained personnel to test attention, memory, processing speed, verbal fluency, and executive functioning. The neuropsychological testing battery included the animal naming test (Lezak et al., 2012), the Rey-Osterrieth Complex Figure Test (CFT) (including immediate recall and delayed recall) (Meyers and Meyers, 1995), the WAIS-III Digit Span and WAIS-III Symbol Coding test (Wechsle, 2012), the WHO-UCLA Auditory Verbal Learning Test (AVLT) (difference of trials 1 to trails 5) (Maj et al., 1993), and the Trail Making Test A and B (TMT) (Lezak et al., 2012). The Rey-15 (Rey, 1964) was used as a brief test of participants' effort. Details on the neuropsychological test battery are described in Bowler et al., 2018. Briefly, the Rey-O Copy trial, participants are tasked with replicating a detailed figure, a task that demands logical thinking and strategic planning, key elements of executive functioning. The Immediate (after a 3-minute interval) and Delayed (after a 30-minute interval) Recall phases of the Rey-O test are utilized to evaluate visuospatial memory capabilities. The

Digit Span test requires examinees to repeat increasing sequences of numbers in the same (forward) and reverse (backward) order. The easier forward task is a measure of sustained attention, and the more effortful backward task includes a working memory component of storing the numbers and letters and alternating them in sequence. The Digit Symbol Coding test measures the speed of processing visual information, short-term visual memory, and the ability to scan visually. Participants are tasked with replicating symbols that correspond to numbers according to a provided key. The WHO-UCLA AVLT test is a verbal learning and retention test involving 15 words from common categories like body parts, read in the same order across five learning trials. This is followed by a disruptive list (List B) in the sixth trial and a recall of the original list in the seventh trial. The difference in scores between the first and fifth trials indicates the learning progress (Lezak et al., 2012). The Trails A test involves quickly scanning and tracking visually, requiring the participant to connect a series of numbered circles in sequential ascending order. Part B of the Trail Making Test demands that participants alternate between connecting circles labeled with consecutive numbers and letters. This task not only involves intricate visual scanning but also cognitive adaptability.

2.3. MRI acquisition

MRI scans were performed on a 3T GE Signa MRI scanner with an 8-channel head coil. A 3D high-resolution T1-weighted sequence was acquired using a fast-spoiled gradient-recalled echo sequence (FSPGR, TR/TE: 6.54/2.8 ms, flip angle: 12°, matrix: 256×256, 220 slices per volume, resolution: $0.9{\times}0.9{\times}1$ mm^3). T1 mapping was achieved using a 3D spoiled gradient echo sequence using a variable flip angle (VFA) method with two echoes (SPGR, TR/TE: 6.36/1.76 ms, flip angles α: 3°, 17°, resolution: $1{\times}1{\times}2$ mm^3) and inversion-recovery SPGR acquisition (IR-PGR, TR/TE/IR = 6.36/1.76/250 ms, flip angle α: 3°, resolution: $1{\times}1{\times}2$ mm^3) to provide a robust correction of flip angle variations. This method is also known as Driven Equilibrium Single Pulse Observation of T1 with High-Speed Incorporation of RF field Inhomogeneities (DESPOT1-HIFI) (Deoni, 2007).

2.4. R1 maps generation

R1 maps were derived from the series of two SPGR scans as described above. The IR-SPGR scan was used to correct for flip angle variations. The fitting procedure was performed using a customized MATLAB (MathWorks, Natick, MA, USA) code (https://github.com/mjt320/HIFI), which generates T1, R1, and B1 maps in addition to other useful parameters such as an estimate of equilibrium signal, S_0, and confidence intervals for R1. Fig. 1 illustrates the input and output of this pipeline. See Supplementary Material for a detailed description of the DESPOT1-HIFI method that was used to generate the R1 maps.

2.5. Voxel-based quantification (VBQ) analyses

Once all of the R1 maps were generated, they were manually aligned to the Montreal Neurological Institute (MNI) T1-weighted 152 template to improve the accuracy of subsequent non-linear transformation to MNI space using the diffeomorphic registration algorithm (DARTEL) (Ashburner, 2007) implemented in SPM12 (www.fil.ion.ucl.ac.uk/spm). The T1-weighted images were also manually aligned to the MNI-152 T1-weighted template and the individual R1 maps were then coregistered to the T1-weighted images from the same subject with the normalized mutual information algorithm. Next, the T1-weighted

images were segmented into grey matter (GM), white matter (WM) and cerebrospinal fluid (CSF) using tissue probability maps (TPMs) specifically derived from multi-parametric maps (Lorio et al., 2014) GM and WM images were non-linearly transformed to standard MNI space, without modulation, using the DARTEL (Ashburner, 2007) tool, and the transformation matrices were applied to each corresponding R1 map. Next, the R1 maps were smoothed by a Gaussian kernel with FWHM = 6 mm to improve the signal to noise ratio (SNR) for statistical comparisons. All data analyses and processing steps were performed in MATLAB 2019a using SPM12 and its extensions. The workflow for this step is shown in Fig. 2.

Hyperintensities in the T1-weighted images may bias automated segmentation results. Smart et al., 2011 shows it is challenging to use T1-weighted images as segmentation references if hyperintensities occur in the segmented regions. To verify that the whole-brain segmentation was not affected by hyperintensities in the T1-weighted images and to account for any impact of image transformation on the R1 maps, a visual check of the GM and WM images was performed for each subject. Additionally, to ensure consistency throughout post-processing, circular ROIs were manually placed on four bilateral regions, including the globus pallidus, caudate nucleus, putamen, and frontal white matter, in both the original R1 map (before transformation), and in the registered R1 map (after transformation).

Finally, to visualize differences in whole-brain R1 between welders and controls, we performed VBQ using SPM12. Voxel-based two-tailed t-statistics (embedded in the General Linear Model framework) was computed to detect regional effects of Mn exposure between controls and Mn-exposed subjects. The model included age at the time of scan and total intracranial volume (TIV) as covariates. An explicit binary mask of GM/WM was provided to ensure inclusion of the same number of voxels in all analyses. The mask was created by averaging over the T1-w derived GM/WM probability maps using the ImCal tool in SPM12. Initial regional differences were assessed by using an auxiliary uncorrected voxel threshold of $p < 0.005$ with a minimum extent threshold of 50 voxels. To correct for multiple comparisons over the whole volume of the GM/WM, a family-wise error (FWE) correction at $p < 0.05$ was applied. For a descriptive summary of the Mn-exposure related R1 changes we generated a second Mn deposition map depicting voxels with $p < 0.01$ to enable a smoother visualization of Mn-deposition in white matter tracts connecting the brain areas with high Mn content found in the $p < 0.005$ map.

2.6. Statistical analysis of associations

To assess the relationship between exposure, motor and cognitive outcomes and R1 values (proxy of Mn deposition), we performed whole-brain voxel-wise correlation tests in SPM12. Because only the welder group is exposed to Mn, we only tested for correlations in the welder group. In welders only, multivariate linear regression was used to test for associations between R1 in each voxel and neuropsychological test scores as well as exposure indices, with age and education level as covariates. The statistical significance level was set to the family-wise error (FWE)-corrected $p < 0.05$ at the cluster-wise level. All the neuropsychological test scores used in statistical analysis were raw scores. For each neuropsychological test and for each CEI, a map representing the correlations with R1 was

calculated with voxels passing the threshold of $p < 0.005$ and a minimum cluster size of 50 voxels. The R1 values in the location of the max T-score (cluster location) were extracted for each subject to run the linear regression model separately and demonstrate the relatedness between the two variables in the form of a scatter plot instead of a statistical map overlaid onto a brain image.

2.7. Data and code availability statement

The data related to this article is not publicly available yet, but the methodology makes use of a publicly available toolbox (SPM12, www.fil.ion.ucl.ac.uk/spm). The standardized procedures (tissue segmentation, DARTEL, voxel-based quantification) within this toolbox were followed. Matlab script for relaxometry maps is publicly available on GitHub (https://github.com/mjt320/HIFI). The only modifications to this script were the parameters for our MRI acquisition (e.g., echo times, flip angles, inversion recovering time).

3.   Results

3.1.   Comparison of ROI-based and whole-brain R1 analysis

A comparison between R1 values extracted from manually placed ROIs in the native space and from the whole-brain Mn deposition map is listed in Table 2, showing excellent agreement of mean R1 values for similar brain regions. This also confirms that R1 was not dramatically changed due to image transformation, as the ROI analysis was done on R1 maps in native space, whereas the whole-brain analysis requires transformations of the R1 maps to a normalized brain.

3.2.   Brain regions showing group differences in Mn deposition

Welders have significantly higher R1 values compared to controls, as shown in a statistical parametric map (Fig. 3). The map represents t-scores as a proxy for excess Mn in welders' brains, as depicted by red (low excess Mn) and yellow (high excess regions) regions, by applying the most stringent criteria $(p < 0.005$ and a minimum cluster size of 50 voxels). Our results show statistically significant higher R1 values in the following bilateral brain regions: parietal operculum, middle frontal gyrus, angular gyrus, and lateral occipital cortex. These brain areas are primarily associated with motor and cognitive functions. Brain structures that were only significant in the left hemisphere (after FWE correction) include the globus pallidus, superior parietal lobule, planum temporale, middle temporal gyrus, postcentral gyrus, and supramarginal and inferior frontal gyrus. Overall, Mn deposition was found to be asymmetric, with more brain areas showing significant changes in the left hemisphere of welders. Detailed information of brain regions that were found to have significantly elevated R1 in our study is listed in Table 3. Table 3 provides specific locations of brain regions (i.e., MNI coordinates) for the right (R) and left (L) hemispheres, along with the maximum (peak) t-value of single voxels within the cluster passing a threshold of $p < 0.005$ and a minimum cluster size of 50 voxels. A high peak t-value (bright yellow) indicates higher significance of the group difference in the voxel. The table also indicates whether the brain regions belong to cognitive or motor networks.

3.3. Manganese accumulation along white matter tracts and the cerebellum

Based on the trends seen in Fig. 3, we performed a secondary analysis by setting the significance threshold to $p < 0.01$ (no cluster minimum) for the depiction of higher R1 brain areas. These auxiliary results show Mn accumulation along white matter tracts and the cerebellum in the human brain. An overlay of the Mn deposition map ($p < 0.01$, uncorrected) onto white matter tracts in a normalized brain is shown in Fig. 4. This secondary analysis showed increased R1 in several white matter tracts, including the external capsule, superior longitudinal fasciculus (SLF), posterior corona radiata, the retrolenticular (part of the internal capsule), the posterior thalamic radiation white matter tracts, the arcuate fasciculus, and the cerebellum. In more detail, elevated R1 was found along the third part of the superior longitudinal fasciculus (SLF III; see Fig. 5A), which connects the motor cortex to the inferior parietal lobe. Pathways showing increased Mn deposition include the retrolenticular part of the internal capsule, localized between the lentiform nucleus and the temporal lobe and the posterior part of the internal capsule connecting to the superior corona radiate and further to the motor cortex. Another white matter tract structure showing increased intensities is the external capsule, which is responsible for connecting the cerebral cortex to other cortical areas and serves as the route for cholinergic fibers from the basal forebrain to the cerebral cortex. Increased R1 was found in the arcuate fasciculus, connecting the superior temporal gyrus to the dorsal prefrontal cortex. Lasty, elevated R1 was also found in the cortex and some white matter areas in the cerebellum (Fig. 5C).

3.4. Associations with exposure and motor and cognitive testing

We found significant positive correlations ($p < 0.005$, FWE corrected), at the cluster-wise level, between R1 and exposure as well as between R1 and increased UPDRS scores in welders. In the cerebellum and frontal cortex, R1 was positively correlated with Mn exposure over the past-3-months ($Mn - CEI_{3M}$) and 7–12 months ($Mn - CEI_{7-12M}$) before the MRI scan as determined by our exposure model for each subject (see Fig. 6) (Ward et al., 2018). No correlations with cumulative exposure since age 18 ($Mn - CEI_{Life}$) was found in this cohort. On average, welders displayed higher UPDRS scores than controls, although not statistically significant when correcting for age and education level (p = 0.178). However, R1 values in the cerebellum and hippocampus were found to be positively correlated with UPDRS scores.

No correlations were found between cognitive tests and elevated R1 over the whole brain in the welder group. A detailed list of all brain regions that have significant associations between increased R1 with exposure and motor function is shown in Table 4. The R1 values in the location of the max T-score (cluster location) were extracted for each subject to run the linear regression model separately to demonstrate the relatedness between the two variables. The results are presented in the table caption as correlation coefficients (r) and slope of the line (β). A plot of the correlation between the most significant voxel value for Mn Past 3-months (CEI_{3M}) vs R1 in the cerebellum white matter is shown in Fig. 6C.

4. Discussion

4.1. Mn distribution

Our study uses a statistical parametric map to represent differences in excess Mn accumulation (as represented by differences in R1) in the brain between welders and controls. The map from our cohort showed widespread increase of R1 in the welders, in both grey matter and white matter, thus underlining the nature of Mn diffusion in the brain. Our parametric maps show prominent Mn accumulation in the bilateral basal ganglia, but no strong link between basal ganglia R1 and exposure metrics, contrasting with other studies (Ma et al., 2018; Lee et al., 2018; Criswell et al., 2019; Criswell et al., 2012; Baker et al., 2015; Lewis et al., 2016). This discrepancy might stem from the different exposure metrics and imaging markers used, but also the fact that our welding cohort includes welders at low and varying exposure levels. We reported previously a lack of association between R1 obtained from a ROI analysis in the globus pallidus with exposure metrics in this same cohort Ma et al., 2018. Evidence from other studies suggest that a certain threshold of exposure must be reached before clear associations between exposure and R1 in the brain show (Ma et al., 2018; Lee et al., 2015; Edmondson et al., 2020). Manganese can cross the BBB using the transferrin-receptor mediated endocytosis, which is highly expressed in the basal ganglia (Rabin et al., 1993). This makes these regions more susceptible to manganese accumulation. Other transporters such as the transporter 1 (DMT1) and ferroportin-1 (FPN1) are also found in the basal ganglia and have roles in cellular manganese uptake and export (Aschner and Gannon, 1994; Aschner and Aschner, 1991). However, the transportation of Mn across the BBB via DMT-1 is a subject of debate. This is due to evidence suggesting that the blood's pH could adversely affect Mn transfer, and that DMT-1 may not be present in the capillary endothelial cells constituting the BBB, as indicated by Crossgrove JS and Yokel RA (Crossgrove and Yokel, 2004). Furthermore, the basal ganglia has a higher energy demand and metabolic activity which can influence the transport and accumulation of metals (Prohaska, 1987) such as Fe and Mn (both share similar chemical properties and transporters). Since none of the examined subjects showed any clinical symptoms of early "manganism", we hypothesize that our data likely reflect pre-symptomatic Mn distribution in the brain.

We observed that a significant difference of Mn deposition in welders compared to controls was shown in both gray matter and white matter. Based on our auxiliary results, gray matter regions showing Mn accumulation were connected via white matter tracts that also showed Mn accumulation, which might suggest a diffusion process of Mn along the white matter tracts. It is well known that Mn can enter active neurons via voltage-gated calcium channels and is transported via microtubule motors down their axons by fast axonal transport (Bearer et al., 2022). In fact, Mn has been used as a contrast agent for magnetic resonance imaging (MRI) studies to map WM tracts in animal models for many years, a technique referred to as manganese-enhanced MRI, or MEMRI (Pautler et al., 1998; Sloot and Gramsbergen, 1994; Watanabe et al., 2001). With our approach of using a whole-brain analysis, our data likely reveals a more complete outline of Mn diffusion and accumulation in white matter tracts such as the superior longitudinal fasciculus, the posterior corona radiata and the external capsule. We also observed high Mn accumulations in areas connecting the motor regulation

network, involving brain areas such as the supramarginal gyrus, anterior corpus callosum and areas surrounding the insula.

The superior longitudinal fasciculus (SLF) is a fiber tract connecting the superior parietal lobe, the inferior parietal lobe, and the supramarginal gyrus, to the frontal and operculum areas (Bruni and Montemurro, 2009). In our results, the third part of the SLF (SLF III) shows increased R1 (Fig. 5A). This fiber connects ventral premotor cortex, inferior frontal gyrus, supramarginal gyrus and the inferior frontal cortex (Stuss and Knight, 2002). In particular, the SLF III has also been linked with somatosensory processing and language, and likely plays a critical role in spatial neglect action (Doricchi et al., 2008), which is one of the symptoms associated with manganism (Bowler et al., 2007) and involves the inability to respond, report, or orient to stimuli. Besides in the SLF, we observed increased R1 also in the supramarginal gyrus, superior temporal lobe, and inferior frontal cortex, all of which are neighboring brain regions to the SLF. Interestingly, and in contrast to symmetric accumulation of Mn in the basal ganglia, Mn accumulation in these cortical areas was significant in the left hemisphere only. Previous research (Stuss and Knight, 2002; Bianchi, 1895; Stuss and Benson, 1984) has suggested that the frontal lobes integrate connected brain regions and modulate the final motor response. Using functional MRI Seo et al. 2016 found that welders had altered neural processing related to executive function in the prefrontal, parietal, and insular cortex under conditions of high cognitive demand. Specifically, welders lacked activation of the insula cortex (Seo et al., 2016), a part of a larger network comprising the lateral prefrontal cortex and parietal cortex. Our report of high Mn accumulation in the brain regions discussed above, including the SLF, would support a possible impairment of frontal-parietal integration in welders as reported in Seo et al., 2016.

Increased Mn accumulation was also found near the arcuate fasciculus (AC), which connects the superior and middle temporal gyrus to the frontal cortex. The AC connects a network associated with auditory function formed by the superior temporal gyrus, superior parietal gyrus, and superior occipital gyrus (Yeatman et al., 2014)

We further found increased Mn deposition in the parietal operculum and the planum temporale (Fig. 5B). The parietal operculum (PO), also known as the secondary somatosensory cortex, is a region located in the parietal lobe of the brain. The PO receives nociceptive projections from the VPI thalamic nuclei and projects into the limbic structure via the insula (Farmer et al., 2018). It plays a crucial role in processing sensory information from various parts of the body, including touch, temperature, and pain (Zilles and Palomero-Gallagher, 2020). The planum temporale (PT) is a region of the temporal lobe (close to Wernicke's area) that is involved in auditory processing and language-related functions (Nakada et al., 2001; Geschwind and Levitsky, 1968). Thus, the excess levels of Mn found in the superior temporal lobe and prefrontal cortex in this study, may explain a negative influence on verbal-IQ reported by Bjørklund et al., 2017 and Bouchard et al., 2018.

4.2. Associations of high R1 with exposure and motor metrics

We found statistically positive correlations of elevated R1 in the cerebellum and the frontal cortex with Mn-CEI$_{3M}$. Both human and animal studies have found that brain Mn as measured by MRI best correlates with exposure over the past-3-months due to its wash-out-

rate (Lee et al., 2015; Edmondson et al., 2019; Lewis et al., 2016; Dorman et al., 2006; Dorman et al., 2006). The finding of increased R1 in the frontal cortex is consistent with a previous longitudinal study which showed that changes in welding hours within 90 days from a scan was associated with changes in R1 after correcting for age, baseline R1, hours worked 90 days before scan, and blood Mn values (Lewis et al., 2016). In our longitudinal study (Edmondson et al., 2019), R1 in the frontal white matter (FWM) increased despite decreased exposure over a period of 2 years. Excess brain Mn in the basal ganglia may have moved to the FWM since the striatum has several connections to the frontal brain. An increase in R1 would result from the anterograde transfer of Mn along axons (Bearer et al., 2022; Pautler et al., 1998; Sloot and Gramsbergen, 1994; Pautler and Koretsky, 2002; Inoue et al., 2011) to the FWM.

4.2.1.   Associations in the frontal cortex—In our results, excess Mn accumulation in the frontal cortex was associated with Mn-CEI$_{3M}$ (see Fig. 6A), which is in line with animal studies that demonstrate the frontal cortex to be a major target of Mn toxicity (Guilarte, 2013; Verina et al., 2013; Guilarte, 2010). Significantly increased Mn has been observed in the frontal cortex of rodents (Elder et al., 2006) and non-human primates after Mn inhalation exposure (Dorman et al., 2006; Bock et al., 2008). In human studies, changes in neurochemical profile have been reported as associated with Mn exposure (Dydak et al., 2011) and verbal learning scores (Chang et al., 2009). Decreased white matter microstructural integrity in welders was found to be associated with subtle motor and cognitive deficits (Kim et al., 2011). These findings suggest that the frontal cortex has an inherent susceptibility to the neurotoxic effects of Mn.

4.2.2.   Associations in the cerebellum—Since this study is analyzing the whole brain, an involvement of the cerebellum in associations between Mn accumulation, exposure and motor function has been detected. Our results show a significant correlation between increased R1 in the cerebellum and Mn-CEI$_{3M}$, and motor function as measured by the UPDRS in welders (Fig. 6B, C). The cerebellum is an essential component of the motor pathway. Little is reported in the literature regarding increased Mn accumulation in the cerebellum and toxic effects in humans. Mn-induced volume decrease has been reported to correlate with reduced performance in fine motor and executive function tasks in full-time welders (Chang et al., 2013). In animal studies, markers of oxidative stress have been identified in the cerebellum (Dobson et al., 2003; Erikson et al., 2004). Connections that are metabolically active and function in both directions have been established between the cerebellum, thalamus, basal ganglia, and cortex (Tobe, 2014). The UPDRS scores are meant to measure clinical motor symptoms in Parkinson's disease. As discussed in detail in Ma et al., 2018 the welders from this cohort displayed only a small non-significant increase in UPDRS scores, which remained within the normal range. However, when the welder group is stratified into high exposure and low exposure groups, significant differences were found.

4.2.3.   Associations in the hippocampus—Lastly, we found a near-significant association between increased R1 in the hippocampus and increased UPDRS scores. Studies in Mn-exposed animals revealed Mn accumulation in the hippocampus, the presence of Aβ diffuse plaques, and deficits in associative learning, the latter being hallmarks of

Alzheimer's disease (AD) or related disorders (Dorman et al., 2006; Guilarte, 2010; Liang et al., 2015). A recent functional MRI study by Burman, 2019 shows that although hippocampal interactions with the motor system are often assumed to reflect the role of memory in motor learning, a specific hippocampal influence on the sensorimotor cortex (SMC) hand representation during volitional movements does not require motor learning. In other words, the hippocampus may control volitional movements and not only motor learning. Furthermore, a recent study by Lee et al., 2019 reports that welders with chronic exposure to Mn have higher mean diffusivity (MD) values in the hippocampus that become greater with increasing age. Overall, these results indicate that the hippocampus may play a role in motor function and microstructural changes related to Mn-induced neurotoxicity.

4.3. Challenges of a whole-brain R1 mapping approach

While diffusion of Mn along axons and its mechanism is well known (Bearer et al., 2022), we also recognize that increased myelination could be another explanation for increased R1 in WM. Increasing myelin content occurs in brain maturation and may be associated with increasing R1 in WM (Eminian et al., 2018; Kühne et al., 2021; Lutti et al., 2014). Animal studies have shown that learning motor skills induces changes in WM microstructure and myelination (Sampaio--Baptista et al., 2013, McKenzie et al., 2014) and several human studies provide evidence that increased myelination plays a central role in WM neuroplasticity improvements during motor learning, (Sale et al., 2017; Reid et al., 2017; Frizzell et al., 2022; Kirby et al., 2022) although this was not shown with R1 mapping but with functional MRI and structural imaging.

While being able to visualize group differences in R1 as whole-brain maps rather than selected regions of interest has clear advantages, several methodological considerations must be made when interpreting the results. First, hyperintensities in the T1-weighted images may bias automated segmentation results as reported by Smart et al., 2011. However, the high signal is the signature of Mn in T1-weighted MRI as reported by Kim, 2004. In our study, we observed in three Mn-exposed subjects hyperintensities in the globus pallidus, putamen, and white matter that were clearly distinguishable by eye. We manually inspected the segmentation results in these three subjects to confirm the results. WM, GM and CSF probability maps were overlaid on T1-weighted images and the segmented results were examined. All three subjects with obvious hyperintensities demonstrated accurate segmentation results according to anatomical landmarks.

Secondly, the values of the R1 map transformed to atlas coordinates should be similar to the values of the original, non-transformed R1 map in native space. Our ROI analysis compared R1 values from regions of interest on the original non-normalized and non-transformed R1-maps with R1 values from the same ROIs on normalized and transformed R1 maps, as necessary for the group comparison. Table 2 shows that these values are highly comparable (correlation coefficients all >0.8), demonstrating the stability of the whole brain analysis in our study. However, diligence should be practiced verifying that Mn deposition maps are not being affected by image transformation due to high Mn exposure.

4.4. Strengths and limitations

The strength of this study is the ability to visualize and assess regional differences in Mn levels across the whole-brain *in vivo*. Our 3D high-resolution maps enable a detailed visualization of the R1 relaxation rate changes as a positive marker of Mn deposition in the deep brain and the cerebral cortex. The R1 whole-brain mapping technique used in this study could be applied to Gadolinium (Gd), another metal that affects R1 in MRI. Growing concerns about the safety of repeated MRI scans with Gd-based contrast agents have emerged due to studies showing Gd accumulation in various brain regions of patients who underwent multiple Gd-based MRI scans (Kanda et al., 2015; McDonald et al., 2015). The developed visualization tool, sensitive to low Mn exposure, could potentially be used to detect low level Gd accumulation in the brain. Furthermore, our automated whole-brain analysis approach could potentially alleviate bias introduced by drawing regional contours for ROIs and may help to reduce uncertainty in the analysis. At this time, this whole-brain R1 mapping approach is only able to show Mn distribution based on group differences. Thus, it shows the extent of Mn depositions for a specific setting of Mn exposure, as e.g., for welders from a particular factory as in this example. To make this tool powerful for individual risk assessment, it will need to be further developed, possibly using a "standard R1 map" as a reference, to allow subject-specific assessment of the distribution of excess brain Mn. Also, this approach was developed using MRI sequences from one MRI vendor and only one method for deriving R1 maps. Future studies that compare the same R1 mapping method across different vendors will be needed to validate this method. Lastly, where we show excess Mn along the white matter tracts, we used a liberal threshold of $p < 0.01$ and did not correct for multiple comparisons. This part of the analysis is rather explorative, aiming to yield new hypotheses for future projects.

5. Conclusions

The development of a whole-brain approach to visualize excess Mn deposition *in vivo* in the human brain allows for a full view of all brain regions affected by exposure to Mn in an occupational study, and further proved that Mn accumulates in many brain regions. Of particular interest is the fact that cortical regions showing significant Mn deposition were connected by white matter tracts also showing significant Mn deposition. Mn accumulation stretching from the lentiform nucleus to motor network structures and cognitive function structures suggests that, with chronic Mn exposure, Mn may diffuse over time from the basal ganglia, or primary accumulation sites, to more distant cortical areas. At the same time, the function of the affected cortical brain regions also correlated with deficits found in motor testing and exposure metrics. Another novel finding is the involvement of the cerebellum, where increased R1 was positively correlated with increased UPDRS (a clinical measure of motor symptoms in Parkinson's disease) and past-3 and 7-12-months exposure. Mn accumulation in the prefrontal cortex, inferior parietal cortex, and middle temporal cortex are consistent with the described neuropsychological impairments in non-human primates and welders, supporting that the location of Mn accumulation affects the function of the corresponding brain networks. Our results show an illustrative view of Mn distribution *in vivo*, suggesting that such Mn maps can be used as a research tool to track the extension of

Mn toxicity in certain exposure settings. The next step towards use in risk assessment would be to develop similar maps on an individual basis.

Supplementary Material

Refer to Web version on PubMed Central for supplementary material.

Acknowledgments

Data availability

Data will be made available on request.

References

Aschner M, Aschner JL, 1991. Manganese neurotoxicity: cellular effects and blood-brain barrier transport. Neuroscience & Biobehavioral Reviews. Pergamon Press plc, pp. 333–340.

Aschner M, Erikson K, 2017. Advanced Nutrition Manganese, 8. American Society for Nutrition, pp. 520–521.

Aschner M, Gannon M, 1994. Manganese (Mn) transport across the rat blood-brain barrier: saturable and transferrin-dependent transport mechanisms. Brain Res. Bull 345–349. [PubMed: 8293318]

Ashburner J, 2007. A fast diffeomorphic image registration algorithm. Neuroimage 38 (1), 95–113. [PubMed: 17761438]

Baker MG, Criswell SR, Racette BA, Simpson CD, Sheppard L, Checkoway H, Sheppard L, 2015. Neurological outcomes associated with low-level manganese exposure in an inception cohort of asymptomatic welding trainees. Scand. J. Work Environ. Health 41 (1), 94–101. Nordic Association of Occupational Safety and Health [PubMed: 25380186]

Bearer EL, Zhang X, Jacobs RE, 2022. Studying axonal transport in the brain by manganese-enhanced magnetic resonance imaging (MEMRI). Methods in Molecular Biology 111–142.

Bjøklund G, Chartrand MS, Aaseth J, 2017. Manganese exposure and neurotoxic effects in children. Environ. Res 155, 380–384. [PubMed: 28282629]

Bock NA, Paiva FF, Nascimento GC, Newman JD, Silva AC., 2008. Cerebrospinal fluid to brain transport of manganese in a non-human primate revealed by MRI. Brain Res. 1198, 160–170. [PubMed: 18243167]

Bouchard MF, Surette C, Cormier P, Foucher D, 2018. Low level exposure to manganese from drinking water and cognition in school-age children. NeuroToxicol. 64, 110–117: Elsevier B.V.

Bowler RM, Roller W, Schulz PE, 2006. Parkinsonism due to manganism in a welder: neurological and neuropsychological sequelae. Neurotoxicology. 27 (3), 327–332. [PubMed: 16457889]

Bowler RM, Lezak MD., 2015. Neuropsychologic evaluation and exposure to neurotoxicants. Handb. Clin. Neurol 23–45.

Bowler RM, Nakagawa S, Drezgic M, Roels HA, Park RM, Diamond E, Mergler D, Bouchard M, Bowler RP, Roller W, 2007. Sequelae of fume exposure in confined space welding: A neurological and neuropsychological case series. Neurotoxicology 28 (2), 298–311. [PubMed: 17169432]

Bowler RM, Roels HA, Nakagawa S, Drezgic M, Diamond E, Park R, Koller W, Bowler RP, Mergler D, Bouchard M, Smith D, Gwiazda R, Doty RL., 2007. Dose-effect relationships between manganese exposure and neurological, neuropsychological and pulmonary function in confined space bridge welders. Occup. Environ. Med 64 (3), 167–177. [PubMed: 17018581]

Bowler RM, Yeh CL, Adams SW, Ward EJ, Ma RE, Dharmadhikari S, Snyder SA, Zauber SE, Wright CW, Dydak U, 2018. Association of MRI T1 relaxation time with neuropsychological test performance in manganese- exposed welders. NeuroToxicol. 64, 19–29: Elsevier B.V.

Bruni JE, Montemurro DG, 2009. Human Neuroanatomy: A Text, Brain Atlas, and Laboratory Dissection Guide. Oxford University Press.

Burman DD., 2019. Hippocampal connectivity with sensorimotor cortex during volitional finger movements: Laterality and relationship to motor learning. PLoS One 14 (9). Public Library of Science.

Chang Y, Jin SU, Rim Y, Shin KM, Lee HJ, Rim SH, Ahn JH, Park SJ, Jeong KS, Weon YC, Lee H, 2013. Decreased brain volumes in manganese-exposed welders. NeuroToxicol. 37, 182–189. Elsevier B.V.;.

Chang Y, Woo ST, Kim Y, Lee JJ, Song HJ, Lee HJ, Rim SH, Lee H, Kwon YJ, Ahn JH, Park SJ, Chung IS, Jeong KS., 2010. Pallidal index measured with three-dimensional T1-weighted gradient echo sequence is a good predictor of manganese exposure in welders. J. Magn. Reson. Imaging 31 (4), 1020–1026. [PubMed: 20373449]

Chang Y, Woo ST, Lee JJ, Song HJ, Lee HJ, Yoo DS, Kim SH, Lee H, Kwon YJ, Ahn HJ, Ahn JH, Park SJ, Weon YC, Chung IS, Jeong KS, Rim Y, 2009. Neurochemical changes in welders revealed by proton magnetic resonance spectroscopy. Neurotoxicology 30 (6), 950–957. [PubMed: 19631686]

Choi DS, Kim EA, Cheong HK, Khang HS, Ryoo JW, Cho JM, Sakong J, Park I, 2007. Evaluation of MR signal index for the assessment of occupational manganese exposure of welders by measurement of local proton T1 relaxation time. Neurotoxicology 28 (2), 284–289. [PubMed: 16828869]

Criswell SR, Nielsen SS, Warden MN, Flores HP, Lenox-Krug J, Racette S, Sheppard L, Checkoway H, Racette BA, 2019. MRI signal intensity and parkinsonism in manganese-exposed workers. J. Occup. Environ. Med 61 (8), 641–645: Lippincott Williams and Wilkins; [PubMed: 31348423]

Criswell SR, Perlmutter JS, Huang JL, Golchin N, Flores HP, Hobson A, Aschner M, Erikson KM, Checkoway H, Racette BA, 2012. Basal ganglia intensity indices and diffusion weighted imaging in manganese-exposed welders. Occup. Environ. Med 69 (6), 437–443. [PubMed: 22447645]

Crossgrove J, Zheng W, 2004. Manganese toxicity upon overexposure. NMR Biomed. 17 (8), 544–553. [PubMed: 15617053]

Crossgrove JS, Yokel RA, 2004. Manganese distribution across the blood–Brain barrier III: the divalent metal transporter-1 is not the major mechanism mediating brain manganese uptake. Neurotoxicology 25 (3), 451–460. [PubMed: 15019308]

Dietz MC, Ihrig A, Wrazidlo W, Bader M, Jansen O, Triebig G, 2001. Results of magnetic resonance imaging in long-term manganese dioxide-exposed workers. Environ. Res 37–40.

Dobson AW, Weber S, Dorman DC, Lash LK, Erikson KM, Aschner M, 2003. Oxidative stress is induced in the rat brain following repeated inhalation exposure to manganese sulfate. Biol. Trace Elem. Res 93 (1), 113–125. [PubMed: 12835496]

Doricchi F, Thiebaut de Schotten M, Tomaiuolo F, Bartolomeo P, 2008. White matter (dis)connections and gray matter (dys)functions in visual neglect: Gaining insights into the brain networks of spatial awareness. Cortex 44 (8), 983–995: Masson SpA; [PubMed: 18603235]

Dorman DC, Struve MF, Marshall MW, Parkinson CU, James RA, Wong BA, 2006. Tissue manganese concentrations in young male rhesus monkeys following subchronic manganese sulfate inhalation. Toxicol. Sci 92 (1), 201–210. [PubMed: 16624849]

Dorman DC, Struve MF, Wong BA, Dye JA, Robertson ID, 2006. Correlation of brain magnetic resonance imaging changes with pallidal manganese concentrations in rhesus monkeys following subchronic manganese inhalation. Toxicol. Sci 92 (1), 219–227. [PubMed: 16638924]

Dydak U, Jiang YM, Long LL, Zhu H, Chen J, Li WM, Edden RAE, Hu S, Fu X, Long Z, Mo XA, Meier D, Harezlak J, Aschner M, Murdoch JB, Zheng W, 2011. *In vivo* measurement of brain GABA concentrations by magnetic resonance spectroscopy in smelters occupationally exposed to manganese. Environ. Health Perspect 119 (2), 219–224. [PubMed: 20876035]

Edmondson DA, Ma RE, Yeh CL, Ward E, Snyder S, Azizi E, Zauber SE, Wells EM, Dydak U, 2019 1. Reversibility of neuroimaging markers influenced by lifetime occupational manganese exposure. Toxicol. Sci 172 (1), 181–190. [PubMed: 31388678]

Edmondson DA, Yeh CL, Hélie S, Dydak U, 2020. Whole-brain R1 predicts manganese exposure and biological effects in welders. Arch. Toxicol 94 (10), 3409–3420. Springer Science and Business Media Deutschland GmbH; [PubMed: 32875357]

Elder A, Gelein R, Silva V, Feikert T, Opanashuk L, Carter J, Potter R, Maynard A, Ito Y, Finkelstein J, Oberdörster G, 2006. Translocation of inhaled ultrafine manganese oxide particles to the central nervous system. Environ. Health Perspect 114 (8), 1172–1178. [PubMed: 16882521]

Eminian S, Hajdu SD, Meuli RA, Maeder P, Hagmann P, 2018. Rapid high resolution T1 mapping as a marker of brain development: Normative ranges in key regions of interest. PLoS ONE 13 (6). . Public Library of Science;

Erikson KM, Dorman DC, Lash LH, Dobson AW, Aschner M, 2004. Airborne manganese exposure differentially affects end points of oxidative stress in an age-and sex-dependent manner. Biol. Trace Elem. Res 100 (1), 49–62. [PubMed: 15258319]

Farmer AD, Ruffle JK, Aziz Q, 2018. Brain processing of gastrointestinal sensory signaling. Physiology of the Gastrointestinal Tract Sixth Ed. Elsevier, pp. 373–385.

Frizzell TO, Phull E, Khan M, Song X, Grajauskas LA, Gawryluk J, D'Arcy RCN, 2022. Imaging functional neuroplasticity in human white matter tracts. Brain Struct. Funct 227 (1), 381–392. . Springer Science and Business Media Deutschland GmbH;. [PubMed: 34812936]

Geschwind N, Levitsky W, 1968. Human brain: left-right asymmetries in temporal speech region. Science 161 (3837), 186–187. [PubMed: 5657070]

Goetz CG, Tilley BC, Shaftman SR, Stebbins GT, Fahn S, Martinez-Martin P, Poewe W, Sampaio C, Stern MB, Dodel R, Dubois B, Holloway R, Jankovic J, Kulisevsky J, Lang AE, Lees A, Leurgans S, LeWitt PA, Nyenhuis D, Olanow CW, Rascol O, Schrag A, Teresi JA, van Hilten JJ, LaPelle N, Agarwal P, Athar S, Bordelan Y, Bronte-Stewart HM, Camicioli R, Chou K, Cole W, Dalvi A, Delgado H, Diamond A, Dick JP, Duda J, Elble RJ, Evans C, Evidente VG, Fernandez HH, Fox S, Friedman JH, Fross RD, Gallagher D, Goetz CG, Hall D, Hermanowicz N, Hinson V, Horn S, Hurtig H, Kang UJ, Kleiner-Fisman G, Klepitskaya O, Kompoliti K, Lai EC, Leehey ML, Leroi I, Lyons KE, McClain T, Metzer SW, Miyasaki J, Morgan JC, Nance M, Nemeth J, Pahwa R, Parashos SA, Schneider J, Schrag A, Sethi K, Shulman LM, Siderowf A, Silverdale M, Simuni T, Stacy M, Stern MB, Stewart RM, Sullivan K, Swope DM, Wadia PM, Walker RW, Walker R, Weiner WJ, Wiener J, Wilkinson J, Wojcieszek JM, Wolfrath S, Wooten F, Wu A, Zesiewicz TA, Zweig RM, 2008. Movement disorder society-sponsored revision of the Unified Parkinson's disease rating scale (MDS-UPDRS): Scale presentation and clinimetric testing results. Mov. Disord 23 (15), 2129–2170. [PubMed: 19025984]

Guilarte TR, Chen MK, McGlothan JL, Verina T, Wong DF, Zhou Y, Alexander M, Rohde CA, Syversen T, Decamp E, Koser AJ, Fritz S, Gonczi H, Anderson DW, Schneider JS, 2006. Nigrostriatal dopamine system dysfunction and subtle motor deficits in manganese-exposed non-human primates. Exp. Neurol 202 (2), 381–390. [PubMed: 16925997]

Guilarte TR, Gonzales KK, 2015. Manganese-induced parkinsonism is not idiopathic Parkinson's disease: Environmental and genetic evidence. Toxicol. Sci 146 (2), 204–212. [PubMed: 26220508]

Guilarte TR, McGlothan JL, Degaonkar M, Chen MK, Barker PB, Syversen T, Schneider JS, 2006. Evidence for cortical dysfunction and widespread manganese accumulation in the nonhuman primate brain following chronic manganese exposure: A 1H-MRS and MRI study. Toxicol. Sci 94 (2), 351–358. [PubMed: 16968886]

Guilarte TR, 2010. APLP1, Alzheimer's-like pathology and neurodegeneration in the frontal cortex of manganese-exposed non-human primates. Neurotoxicology 31 (5), 572–574. [PubMed: 20188756]

Guilarte TR, 2013. Manganese neurotoxicity: New perspectives from behavioral, neuroimaging, and neuropathological studies in humans and non-human primates. Front. Aging Neurosci 5 (JUN).

Inoue T, Majid T, Pautler RG, 2011. Manganese enhanced MRI (MEMRI): Neurophysiological applications. Rev. Neurosci 22 (6), 675–694. [PubMed: 22098448]

Jiang Y, Zheng W, Long L, Zhao W, Li X, Mo X, Lu J, Fu X, Li W, Liu S, Long Q, Huang J, Pira E, 2007. Brain magnetic resonance imaging and manganese concentrations in red blood cells of smelting workers: Search for biomarkers of manganese exposure. Neurotoxicology 28 (1), 126–135. [PubMed: 16978697]

Kanda T, Fukusato T, Matsuda M, Toyoda K, Oba H, Kotoku J, Haruyama T, Kitajima K, Furui S, 2015. Gadolinium-based contrast agent accumulates in the brain even in subjects without severe

renal dysfunction: Evaluation of autopsy brain specimens with inductively coupled plasma mass spectroscopy. Radiology 276 (1), 228–232. [PubMed: 25942417]

Kim Y, Jeong KS, Song HJ, Lee JJ, Seo JH, Kim GC, Lee HJ, Kim HJ, Ahn JH, Park SJ, Kim SH, Kwon YJ, Chang Y, 2011. Altered white matter microstructural integrity revealed by voxel-wise analysis of diffusion tensor imaging in welders with manganese exposure. Neurotoxicology 32 (1), 100–109. [PubMed: 21111757]

Kim Y, 2004. High signal intensities on T1-weighted MRI as a biomarker of exposure to manganese. Ind. Health 111–115. [PubMed: 15128159]

Kirby ED, Frizzell TO, Grajauskas LA, Song X, Gawryluk JR, Lakhani B, Boyd L, D'Arcy RCN, 2022. Increased myelination plays a central role in white matter neuroplasticity. NeuroImage 263, 119644. [PubMed: 36170952]

Bianchi L, 1895. The functions of the frontal lobes. Brain 18 (4), 497–522. 10.1093/brain/18.4.497.

Krieger D, Krieger S, Theilmann L, Jansen O, Gass P, Lichtnecker H, 1995. Manganese and chronic hepatic encephalopathy. Lancet 346 (8970), 270–274. [PubMed: 7630246]

Kühne F, Neumann WJ, Hofmann P, Marques J, Kaindl AM, Tietze A, 2021. Assessment of myelination in infants and young children by T1 relaxation time measurements using the magnetization-prepared 2 rapid acquisition gradient echoes sequence. Pediatr. Radiol 51, 2058–2068. [PubMed: 34287663]

Lee EY, Flynn MR, Du G, Lewis MM, Fry R, Herring AH, Van Buren E, Van Buren S, Smeester L, Kong L, Yang Q, Mailman RB, Huang X, 2015. T1 relaxation rate (R1) indicates nonlinear mn accumulation in brain tissue of welders with low-level exposure. Toxicol Sci. 146 (2), 281–289. [PubMed: 25953701]

Lee EY, Flynn MR, Du G, Lewis MM, Kong L, Yanosky JD, Mailman RB, Huang X, 2019. Higher hippocampal mean diffusivity values in asymptomatic welders. Toxicol. Sci 168 (2), 486–496. [PubMed: 30629252]

Lee EY, Flynn MR, Lewis MM, Mailman RB, Huang X, 2018. Welding-related brain and functional changes in welders with chronic and low-level exposure. NeuroToxicol. 64, 50–59. . Elsevier B.V.;

Lewis MM, Flynn MR, Lee EY, Van Buren S, Van Buren E, Du G, Fry RC, Herring AH, Kong L, Mailman RB, Huang X, 2016. Longitudinal T1 relaxation rate (R1) captures changes in short-term Mn exposure in welders. NeuroToxicol. 57, 39–44.

Lewis MM, Lee EY, Jo HJ, Du G, Park J, Flynn MR, Kong L, Latash ML, Huang X, 2016. Synergy as a new and sensitive marker of basal ganglia dysfunction: A study of asymptomatic welders. Neurotoxicology 56, 76–85. [PubMed: 27373673]

Liang G, Qin H, Zhang L, Ma S, Huang X, Lv Y, Qing L, Li Q, xiong Y, Huang Y, Chen K, Huang Y, Shen Y, Nong J, Yang X, Zou Y, 2015. Effects of chronic manganese exposure on the learning and memory of rats by observing the changes in the hippocampal cAMP signaling pathway. Food Chem. Toxicol 83, 261–267. [PubMed: 26164403]

Long Z, Dyke JP, Ma R, Huang CC, Louis ED, Dydak U, 2015. Reproducibility and effect of tissue composition on cerebellar γ-aminobutyric acid (GABA) MRS in an elderly population. NMR Biomed. 28 (10), 1315–1323. [PubMed: 26314380]

Lorio S, Lutti A, Kherif F, Ruef A, Dukart J, Chowdhury R, Frackowiak RS, Ashburner J, Helms G, Weiskopf N, Draganski B, 2014. Disentangling *In vivo* the effects of iron content and atrophy on the ageing human brain. NeuroImage 103, 280–289. [PubMed: 25264230]

Lutti A, Dick F, Sereno MI, Weiskopf N, 2014. Using high-resolution quantitative mapping of R1 as an index of cortical myelination. Neuroimage 93, 176–188. [PubMed: 23756203]

Deoni SCL, 2007. High-resolution T1 mapping of the brain at 3T with driven equilibrium single pulse observation of T1 with high-speed incorporation of RF field inhomogeneities (DESPOT1-HIFI). J. Magn. Reson. Imaging 26 (4), 1106–1111. [PubMed: 17896356]

Lezak MD, Howieson DB, Bigler ED, Tranel D, 2012. Neuropsychological Assessment. Oxford University Press, Inc.

Ma RE, Ward EJ, Yeh CL, Snyder S, Long Z, Gokalp Yavuz F, Zauber SE, Dydak U, 2018. Thalamic GABA levels and occupational manganese neurotoxicity: Association with exposure levels and brain MRI. NeuroToxicol. 64, 30–42. . Elsevier B.V.;

Martin KV, Edmondson D, Cecil KM, Bezi C, Vance ML, McBride D, Haynes EN, 2020. Manganese exposure and neurologic outcomes in adult populations. Neurol. Clin 38 (4), 913–936. W.B. Saunders; [PubMed: 33040869]

McDonald RJ, McDonald JS, Kallmes DF, Jentoft ME, Murray DL, Thielen KR, Williamson EE, Eckel LJ, 2015 Jun 1. Intracranial gadolinium deposition after contrast-enhanced MR imaging. Radiology 275 (3), 772–782. [PubMed: 25742194]

McKenzie IA, Ohayon D, Li H, De Faria JP, Emery B, Tohyama K, Richardson WD, 2014. Motor skill learning requires active central myelination. Science 346 (6207), 318–322. . American Association for the Advancement of Science; [PubMed: 25324381]

Meyers JE, Meyers KR, 1995. Rey complex figure test under four different administration procedures. Clin. Neuropsychol 9 (1), 63–67.

Nakada T, Fujii Y, Yoneoka Y, Kwee IL, 2001. Planum temporale: Where spoken and written language meet. Eur. Neurol 121–125. Available from. www.karger.com/journals/ene.

Maj M, D'Elia L, Satz P, Janssen R, Zaudig M, Uchiyama C, Starace F, Galderisi S, Chervinsky A, World Health Organization, Division of Mental Health/Global Programme on AIDS, 1993. Evaluation of two new neuropsychological tests designed to minimize cultural bias in the assessment of HIV-1 seropositive persons: a WHO study. Arch. Clin. Neuropsychol. Off. J. Natl. Acad. Neuropsychol 8 (2), 123–135.

Olanow CW, 2004. Manganese-induced Parkinsonism and Parkinson's disease. Ann. N Y Acad. Sci 1012 (1), 209–223. [PubMed: 15105268]

Pautler RG, Koretsky AP, 2002. Tracing odor-induced activation in the olfactory bulbs of mice using manganese-enhanced magnetic resonance imaging. Neuroimage 16 (2), 441–448. [PubMed: 12030829]

Pautler RG, Silva AC, Koretsky AP, 1998. *In vivo* neuronal tract tracing using manganese-enhanced magnetic resonance imaging. Magn. Reson. Med 40 (5), 740–748. Lippincott Williams and Wilkins; [PubMed: 9797158]

Prohaska JR, 1987. Functions of trace elements in brain metabolism. Physiol. Rev Available from www.physiology.org/journal/physrev.

Rabin O, Hegedus L, Bourre J-M, Smith QR, 1993. Rapid brain uptake of manganese(II) across the blood-brain barrier. J. Neurochem 61 (2), 509–517. [PubMed: 7687654]

Racette BA, Aschner M, Guilarte TR, Dydak U, Criswell SR, Zheng W, 2012. Pathophysiology of manganese-associated neurotoxicity. Neurotoxicology 33 (4), 881–886. [PubMed: 22202748]

Reid LB, Sale MV, Cunnington R, Mattingley JB, Rose SE, 2017. Brain changes following four weeks of unimanual motor training: Evidence from fMRI-guided diffusion MRI tractography. Hum. Brain Mapp 38 (9), 4302–4312. [PubMed: 28677154]

Rey A, 1964. L'examen clinique en psychologie (The Clinical Psychological Examination). Presse Univ Fr Paris.

Sale MV, Reid LB, Cocchi L, Pagnozzi AM, Rose SE, Mattingley JB, 2017. Brain changes following four weeks of unimanual motor training: Evidence from behavior, neural stimulation, cortical thickness, and functional MRI. Hum. Brain Mapp 38 (9), 4773–4787. [PubMed: 28677224]

Sampaio-Baptista C, Khrapitchev AA, Foxley S, Schlagheck T, Scholz J, Jbabdi S, DeLuca GC, Miller KL, Taylor A, Thomas N, Kleim J, Sibson NR, Bannerman D, Johansen-Berg H, 2013. Motor skill learning induces changes in white matter microstructure and myelination. J. Neurosci 33 (50), 19499–19503. [PubMed: 24336716]

Sen S, Flynn MR, Du G, Tröster AI, An H, Huang X, 2011. Manganese accumulation in the olfactory bulbs and other brain regions of "asymptomatic" welders. Toxicol. Sci 121 (1), 160–167. [PubMed: 21307282]

Seo J, Chang Y, Jang KE, Park JW, Kim YT, Park SJ, Jeong KS, Kim A, Kim SH, Kim Y, 2016. Altered executive function in the welders: A functional magnetic resonance imaging study. Neurotoxicol Teratol. 56, 26–34. [PubMed: 27208889]

Shin YC, Kim E, Cheong HK, Cho S, Sakong J, Kim KS, Yang JS, Jin YW, Kang SK, Kim Y, 2007. High signal intensity on magnetic resonance imaging as a predictor of neurobehavioral performance of workers exposed to manganese. Neurotoxicology 28 (2), 257–262. [PubMed: 16647136]

Sloot WN, Gramsbergen JBP, 1994. Axonal transport of manganese and its relevance to selective neurotoxicity in the rat basal ganglia. Brain Res. 657 (1), 124–132. [PubMed: 7820609]

Smart SD, Firbank MJ, O'Brien JT, 2011. Validation of automated white matter hyperintensity segmentation. J. Aging Res 2011.

Stuss DT, Benson DF, 1984. Neuropsychological studies of the frontal lobes. Psychol. Bull 3–28. [PubMed: 6544432]

Stuss DT, Knight RT, 2002. Principles of Frontal Lobe Function. Oxford University Press.

Tobe EH, 2014. Cerebellar dysregulation and heterogeneity of mood disorders. Neuropsychiatr. Dis. Treat 10, 1381–1384. [PubMed: 25092983]

Tsuboi Y, Uchikado H, Dickson DW, 2007. Neuropathology of Parkinson's disease dementia and dementia with Lewy bodies with reference to striatal pathology. Parkinsonism Relat. Disord 13, S221–S224. [PubMed: 18267239]

Verina T, Schneider JS, Guilarte TR, 2013 Mar 3. Manganese exposure induces α-synuclein aggregation in the frontal cortex of non-human primates. Toxicol. Lett 217 (3), 177–183. [PubMed: 23262390]

Ward EJ, Edmondson DA, Nour MM, Snyder S, Rosenthal FS, Dydak U, 2018. Toenail manganese: A sensitive and specific biomarker of exposure to manganese in career welders. Ann Work Expo Health, 62. Oxford University Press, pp. 101–111.

Watanabe T, Michaelis T, Frahm J, 2001. Mapping of retinal projections in the living rat using high-resolution 3D gradient-echo MRI with Mn2+-induced contrast. Magn. Reson. Med 46 (3), 424–429. John Wiley and Sons Inc. [PubMed: 11550231]

Wechsle D, 1997. WAIS-III : administration and scoring manual : wechsler adult intelligence scale. Psychol. Corp [cited 2023 Aug 29]; Available from. https://www.worldcat.org/title/waisiiiadministrationandscoringmanualwechsleradultintelligencescale/oclc/224913150.

Yeatman JD, Wandell BA, Mezer AA, 2014. Lifespan maturation and degeneration of human brain white matter. Nat Commun. 5. Nature Publishing Group;

Zilles K, Palomero-Gallagher N. 4.14 - The Architecture of Somatosensory Cortex. In: Fritzsch B, editor. Senses Compr Ref Second Ed [Internet]. Oxford: Elsevier; 2020 [cited 2024 Jan 24]. p. 225–260. Available from: https://www.sciencedirect.com/science/article/pii/B978012809324524128X.

Zoni S, Albini E, Lucchini R, 2007. Neuropsychological testing for the assessment of manganese neurotoxicity: a review and a proposal. Am. J. Ind. Med 50 (11), 812–830. [PubMed: 17918193]
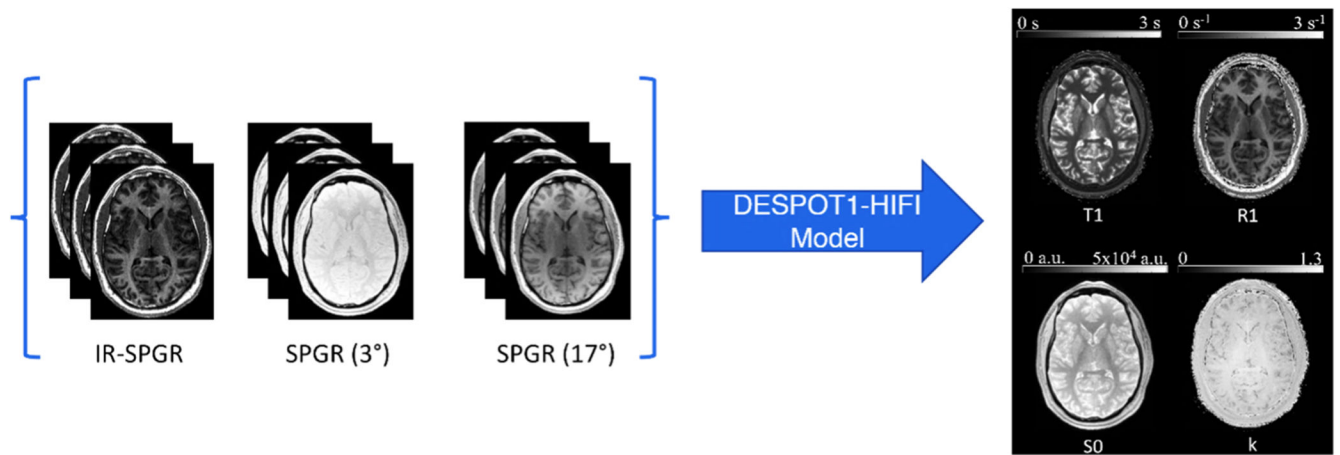
Fig. 1.
DESPOT1-HIFI processing pipeline. Each participant's SPGR images are first co-registered to the IR-SPGR scans to account for motion. Next, from the combined multiangle SPGR and IR-SPGR data, a unique solution for field inhomogeneities, T1, R1 (1/T1), and proton density (S0) can be found through a non-linear least-squares minimization operation on the combined data.
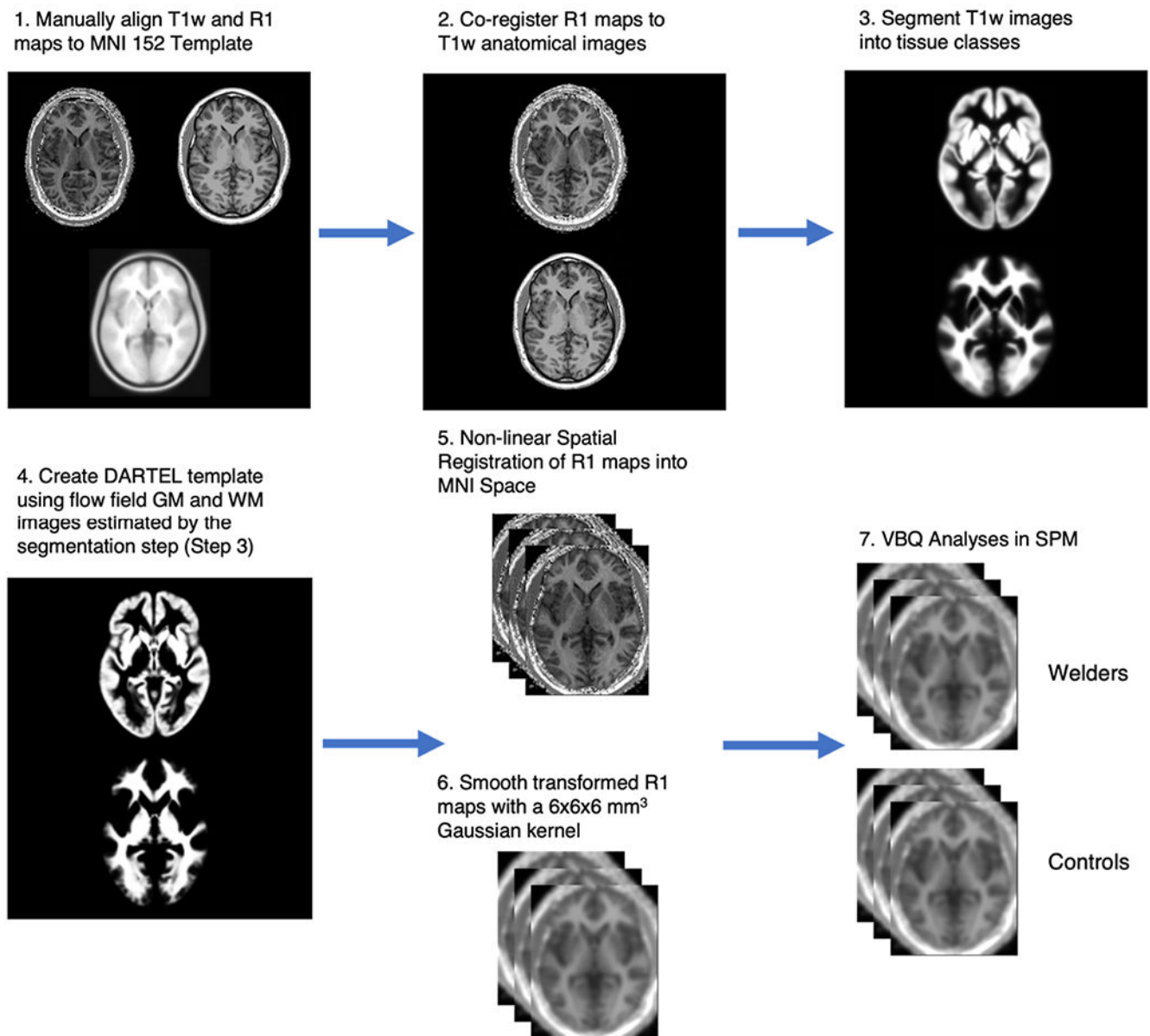
Fig. 2.
Next, the R1 maps and T1-w images were manually aligned to the Montreal Neurological Institute (MNI152) to increase the consistency in individual head positions prior to tissue segmentations and normalization. R1 maps were then co-registered to their corresponding T1-w images to ensure that after segmentation of the T1-w images, the R1 maps can be transformed to the standard space for group-level analysis.
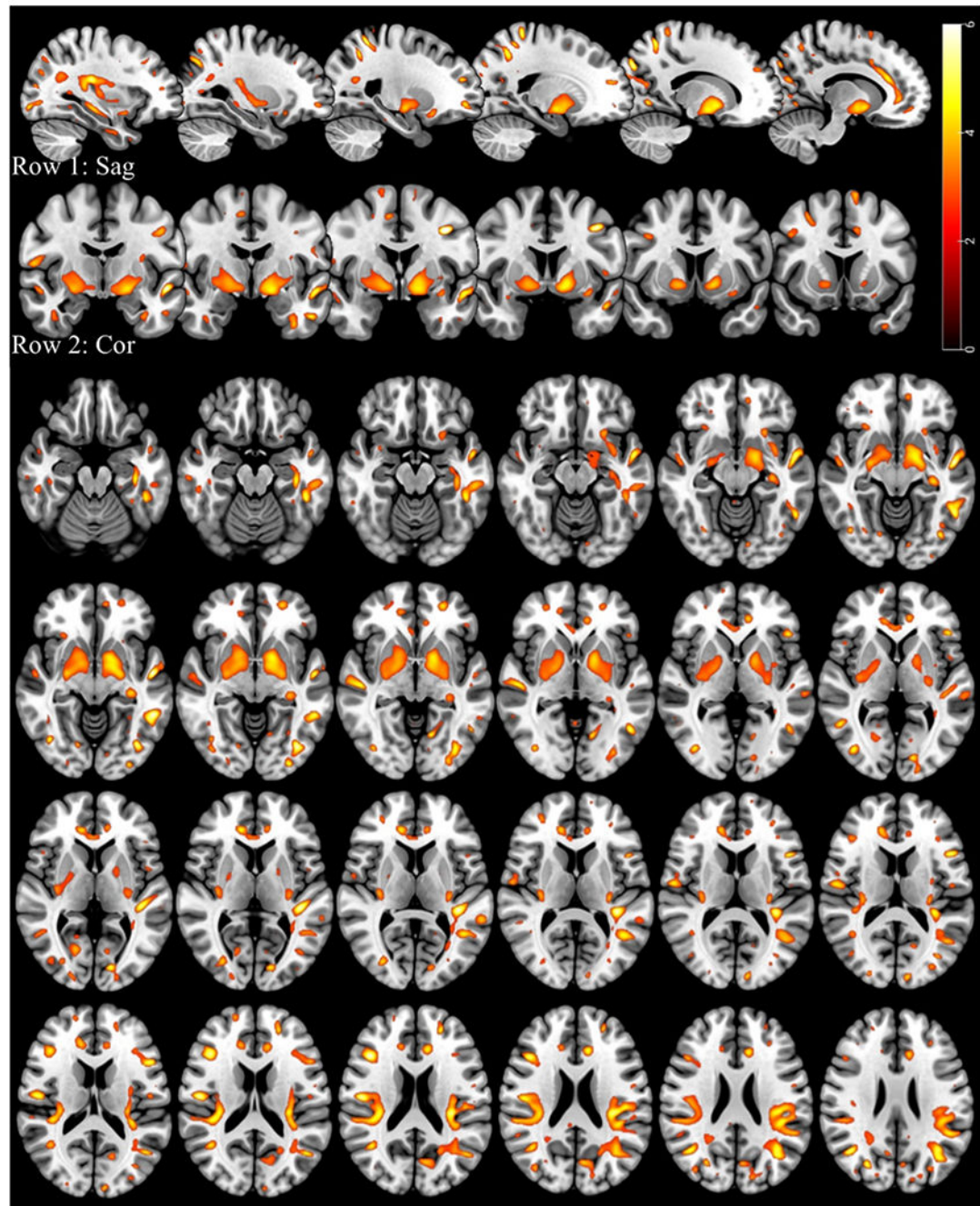
Fig. 3.
Overlay of Mn map ($p < 0.005$, 50 voxels, before FWE correction) with MNI template. Excess Mn deposition maps are shown in sagittal view (row 1), coronal view (row 2), and axial view (rows 3–6). Regions with significantly increased R1 values in the welder group are displayed in yellow-orange color, with the color indicating the exponent of the p-value, T, in the equation $p = 10^{-T}$.
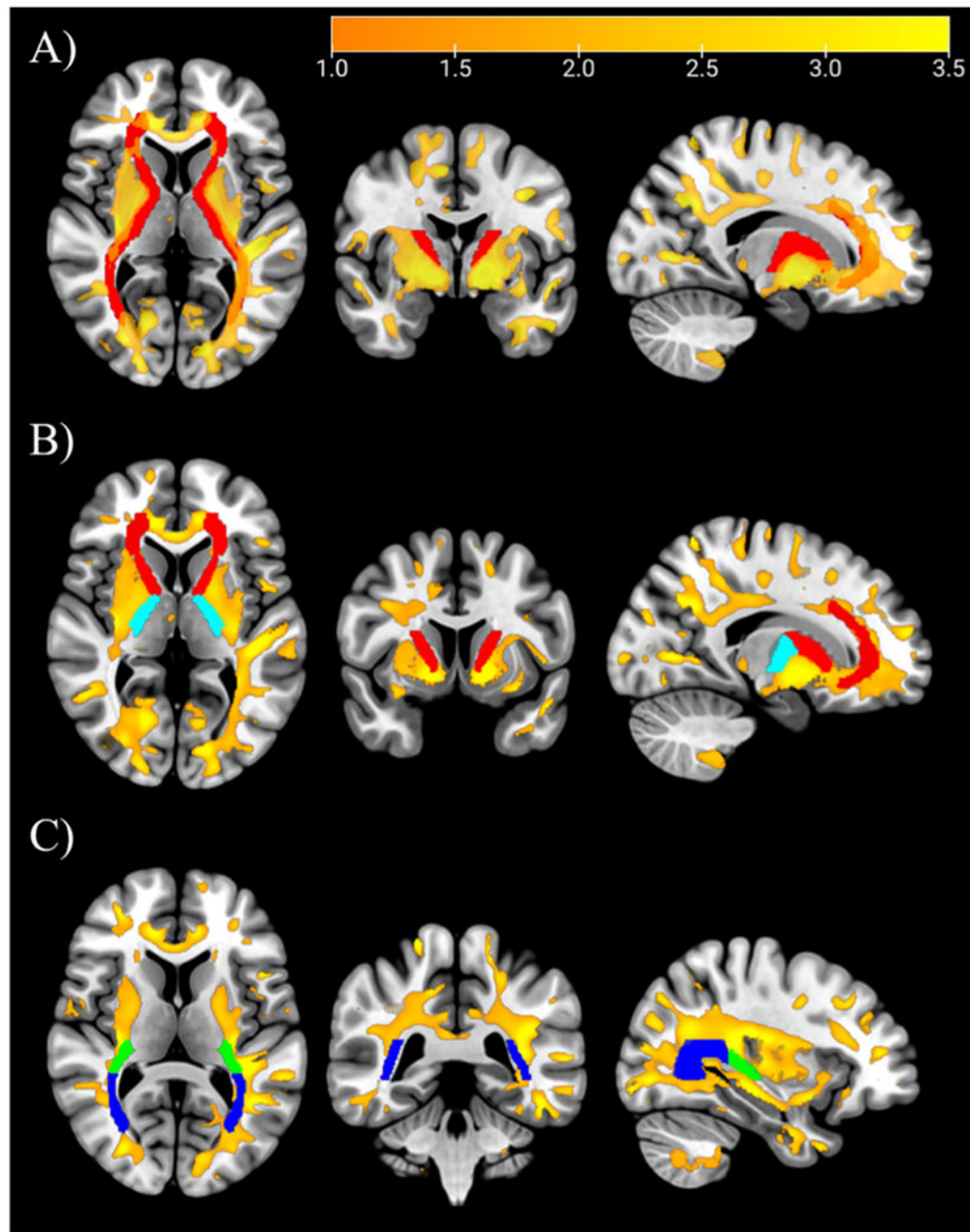
Fig. 4.

Overlay of Mn map (p<0.01, no FWE correction) in yellow-orange onto MNI template. The white matter templates (red, blue green) from top to bottom are A) combined anterior corona radiata, anterior and posterior limbs of the internal capsule, retrolenticular part of internal capsule, and posterior thalamic radiation (includes the optic radiation); B) anterior corona radiata and anterior limb of internal capsule (red) and posterior limb of internal capsule (light blue); C) retrolenticular part of internal capsule (green) and posterior thalamic

radiation (include optic radiation) in blue. Masks are from the JHU DTI-based white-matter atlases. The color bar indicates the exponent of the p-value, T, in the equation $p = 10^{-T}$.
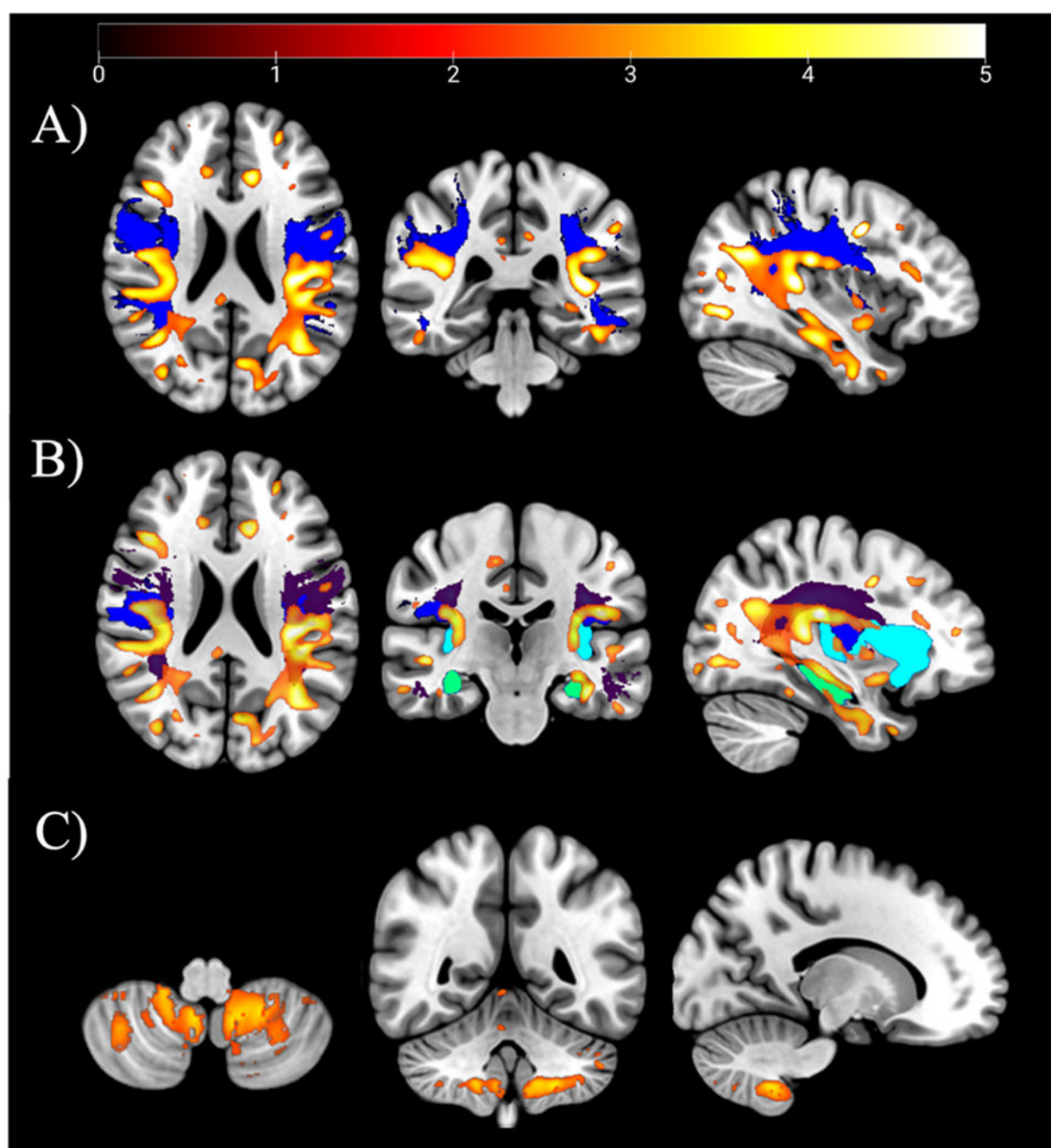
Figure 5.
Overlay of Mn map ($p < 0.01$, no FWE correction) with MNI template showing elevated Mn deposition on A) the superior longitudinal fasciculus, and B) the arcuate fasciculus (purple) white matter tracts, insula (light blue), parietal operculum (blue), the hippocampus (green), and C) the cerebellum. The color bar indicates the exponent of the p-value, T, in the equation $p = 10^{-T}$.
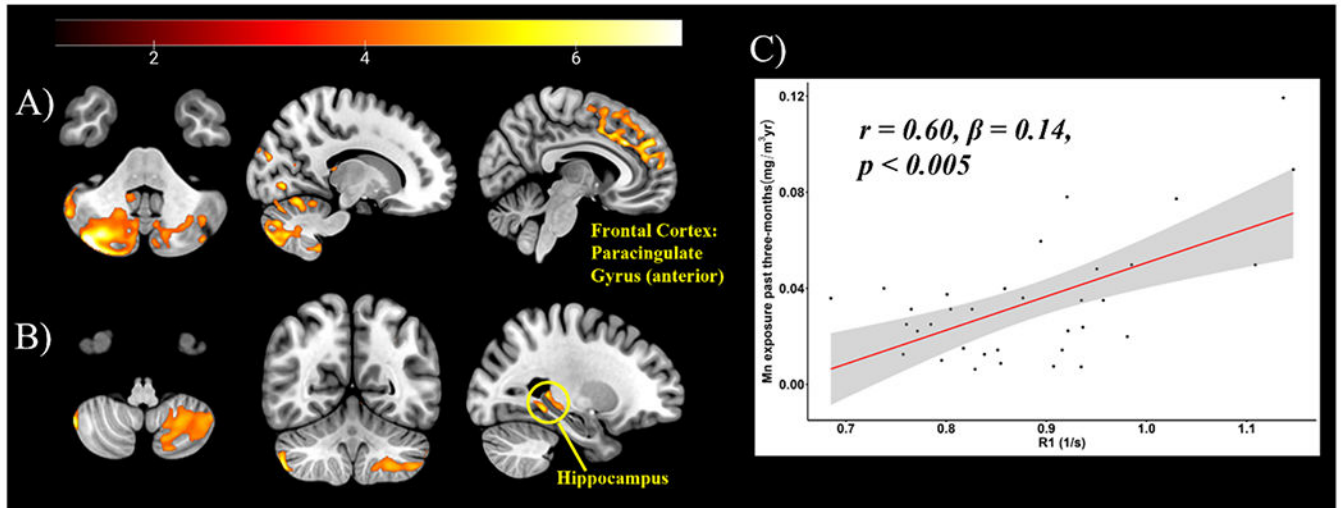
Fig. 6.
Statistical map showing elevated R1 in the cerebellum and frontal cortex correlated with Mn exposure past 3-months, and B) elevated R1 in the cerebellum and hippocampus correlated with higher UPDRS global scores. The color bar indicates the exponent of the p-value, T, in the equation $p = 10^{-T}$. C) Example plot of the correlation between the R1 voxel value (in the cerebellum) and Mn exposure past 3-months at the most significant location.

Table 1

Characteristics of participants included in the analyses.

Characteristics of participants	Welders (n = 36)	Controls (n = 23)
Age (y) [mean ± SD]	39.9 ± 10.7	38.8 ± 11.1
Years of Education (y) [mean ± SD]	12.6 ± 1.3	12.9 ± 1.2
Total intercranial volume (cm^3) [mean ± SD]	1501.7 ± 127.4	1502.9 ± 104.5
Welding years (y) [mean ± SD]	12.5 ± 8.8	0 ± 0
Exposure (mg/m^3·yr) [mean ± SD]		
Mean Airborne Mn Exposure	0.146 ± 0.109	0.003 ± 0.002
Mn cumulative exposure index (Mn-CEI$_{3M}$)	0.038 ± 0.035	0.0005 ± 0.0003
Mn cumulative exposure index (Mn-CEI$_{7-12M}$)	0.074 ± 0.080	0.001 ± 0.001
Mn cumulative exposure index (Mn-CEI$_{Life}$)	1.444 ± 1.292	0.043 ± 0.034

Table 2

Comparison of R1 values acquired from ROI analysis in native space and MNI space.

	Globus Pallidus (1/s) Mean ± SD	Caudate Nucleus (1/s) Mean ± SD	FWM (1/s) Mean ± SD	Putamen (1/s) Mean ± SD
Controls Native Space	1.05 ± 0.07	0.76 ± 0.07	1.42 ± 0.16	0.81 ± 0.06
Controls MNI Space	1.06 ± 0.07	0.75 ± 0.06	1.41 ± 0.15	0.82 ± 0.07
r^2 (p-value)	0.94 (<0.001)	0.75 (<0.001)	0.98 (<0.001)	0.97 (<0.001)
Welders Native Space	1.17 ± 0.16	0.82 ± 0.13	1.57 ± 0.22	0.87 ± 0.13
Welders MNI Space	1.16 ± 0.17	0.81 ± 0.12	1.56 ± 0.22	0.88 ± 0.12
r^2 (p-value)	0.97 (<0.001)	0.97 (<0.001)	0.99 (<0.001)	0.89 (<0.001)

r^2 refers to the Pearson correlation coefficient

Table 3

Summary of voxel-based quantification (VBQ) results within WM/GM (pFWE<0.05) showing elevated Mn deposition throughout the brain. Uncorrected auxiliary results (p<0.005, cluster extend threshold= 50, no FWE correction) are highlighted with an asterisk.

Brain Region	Side	MNI Coordinates[a]			Peak T[b]
		X	**Y**	**Z**	**Value**
Basal Ganglia					
Globus Pallidum	R*	15	6	−6	3.90
	L	−15	5	−6	6.14
Putamen (posterior)*	R	28	−4	−5	3.32
	L	−28	−17	1	3.28
Motor Network Structures					
Precentral Gyrus*	R	12	−20	47	4.06
	L	-	-	-	-
Postcentral Gyrus	R	21	−41	72	4.72
	L	−19	−42	67	5.27
Supramarginal Gyrus	R	-	-	-	-
	L	−52	−46	35	5.39
Angular Gyrus	R	45	−52	35	5.54
	L	−37	−60	25	5.35
Cognitive Function Structures					
Parietal Operculum	R	49	−13	19	6.17
	L	−32	−28	21	5.61
Planum Temporale	R*	56	−9	12	5.52
	L	−38	−35	9	6.39
Superior Temporal Gyrus	R	-	-	-	-
	L	−53	−2	−13	5.99
Inferior Frontal Gyrus	R	-	-	-	-
	L	−49	17	15	5.28
Middle Frontal Gyrus	R	41	24	20	6.14
	L	−38	1	39	8.13
Superior Parietal Lobule	R*	31	−50	40	5.36
	L	−16	−57	57	5.76
White Matter Tracts					
Anterior Corona Radiata*,[c]	R	16	38	8	3.56
	L	−15	33	18	2.81
External Capsule*,[c]	R	−32	−16	1	2.70
	L	33	−16	1	2.93
Superior Longitudinal Fasciculus (III) *,[c]	R	38	−54	15	3.15
	L	−38	−54	15	3.04
Posterior Corona Radiata*,[c]	R	26	−46	27	2.90

Brain Region	Side	MNI Coordinates[a]			Peak T[b]
		X	Y	Z	Value
Arcuate Fasciculus*,[c]	L	−26	−46	27	2.53
	R	36	−32	18	2.70
	L	−36	−55	13	2.93
Retrolenticular (Part of Internal Capsule)*,[c]	R	29	−24	9	3.40
	L	−29	−24	9	2.76
Posterior Thalamic Radiation*,[c]	R	30	−50	23	2.58
	L	−30	−50	23	2.56

[a]Coordinates of the voxel with maximum (peak) t-value inside the corresponding cluster provided in Montreal Neurological Institute (MNI) space.

[b]Peak T is the power in the equation $p = 10^{-T}$. Maximum (peak) t-value of single voxels within the cluster passing a threshold of $p<0.005$ and a minimum of 50 voxels.

[c]White matter tracts. These were identified using the John's Hopkins University (JHU) DTI-based white-matter atlases (https://identifiers.org/neurovault.image:1401).

Table 4

Summary of associations found between increased R1 with exposure and motor function. Mn past-3-months vs Cerebellum White Matter ($r = 0.60$, $\beta = 0.14$); Mn past 7-12-months vs Cerebellum Cortex ($r = 0.21$, $\beta = 0.41$), UPDRS vs Mn in Cerebellum Cortex ($r = 0.44$, $\beta = 9.01$); UPDRS vs Hippocampus ($r = 0.53$, $\beta = 24.7$).

Brain Region	Side	Cluster[a] Size	P[FWE-corr][b]	Coordinates[c] X	Y	Z	Peak T[d] Value
Manganese exposure							
Mn past-3-months (positive correlation)							
Cerebellum Cortex: Cerebellum Exterior		28110	0.000				
	R			39	−79	−42	4.88
	L			−17	−75	−35	4.09
Cerebellum White Matter	R			24	−78	−39	6.63
	L			-	-	-	-
Frontal Cortex Paracingulate Gyrus (anterior)		6998	0.004				
	R			−6	21	39	3.51
	L			3	21	38	4.61
Mn past 7-12-months (positive correlation)							
Cerebellum Cortex: Cerebellum Exterior		119551	0.000				
	R			40	−78	−42	9.71
	L			−20	−79	−79	7.31
Cerebellum White Matter	R			-	-	-	-
	L			−30	−68	−38	6.01
Motor Function							
UPDRS (positive correlation)							
Cerebellum Cortex: Cerebellum Exterior		9173	0.001				
	R			49	−59	−51	5.54
	L			−46	−55	−51	3.96
Medial Temporal Cortex: Hippocampus		1966	0.055				
	R			26	−37	2	N/A
	L			−26	−37	2	5.46

[a] The number of voxels each showing statistically significant association with exposure and motor metrics.

[b] Cluster size p-value, corrected for multiple comparisons using the Family-Wise Error (FWE) rate, that establishes the probability of the occurrence of a cluster of the specified voxel size or larger under the null hypothesis of a brain made of voxels with only spatially autocorrelated noise.

[c] Coordinates of the voxel with maximum (peak) t-value inside the corresponding cluster provided in Montreal Neurological Institute (MNI) space.

*d*Maximum (peak) *t*-value within the cluster. The *t*-values are generated from the voxel-wise regression model.